Dynamic Connectivity in Wireless Underground Sensor Networks

Zhi Sun, *Student Member, IEEE,* Ian F. Akyildiz, *Fellow, IEEE,* and Gerhard P. Hancke, *Senior Member, IEEE,*

Abstract

In wireless underground sensor networks (WUSNs), due to the dynamic underground channel characteristics and the heterogeneous network architecture, the connectivity analysis is much more complicated than in the terrestrial wireless sensor networks and ad hoc networks, which was not addressed before, to our knowledge. In this paper, a mathematical model is developed to analyze the dynamic connectivity in WUSNs, which captures the effects of environmental parameters such as the soil composition and the random soil moisture, and system parameters such as the operating frequency, the sensor burial depth, the sink antenna height, the density of the sensor and sink devices, the tolerable latency of the networks, and the number and the mobility of the above-ground sinks. The lower and upper bounds of the connectivity probability are derived to analytically provide principles and guidelines for the design and deployment of WUSNs in various environmental conditions.

Index Terms

Dynamic Connectivity, Wireless Underground Sensor Networks, Soil Medium.

I. Introduction

Wireless Underground Sensor Networks (WUSNs) are networks of sensor nodes that are buried underground and communicate through soil. WUSNs enable a wide variety of novel applications, such as intelligent agriculture, smart underground power grid, in-situ sensing for oil recovery, border patrol, sports field maintenance, among others [1], [2], [4], [5]. Since the underground

Zhi Sun and Ian F. Akyildiz are with the Broadband Wireless Networking Laboratory, School of Electrical and Computer Engineering, Georgia Institute of Technology, Atlanta, GA, 30332, United States. E-mail: {zsun; ian}@ece.gatech.edu

Gerhard P. Hancke is with Department of Electrical, Electronic & Computer Engineering University of Pretoria, South Africa, 0002. E-mail: g.hancke@ieee.org

A shorter version of this paper appeared in [3].

sensor nodes are expected to transmit sensing data to one or multiple aboveground data sinks via single or multi-hop paths, the connectivity in WUSNs is essential for the system functionalities.

Because of the complex channel characteristics and the heterogeneous network architecture, the connectivity analysis in the WUSNs is much more complicated than in the terrestrial wireless sensor networks. In particular, since the WUSNs consist of underground (UG) sensor nodes and aboveground (AG) sinks [1], [6], [7], three different communication channels exist in WUSNs, including: underground-to-underground (UG-UG) channel, underground-to-aboveground (UG-AG) channel, and aboveground-to-underground (AG-UG) channel. The transmission range in these three different channels is dramatically different from each other and are significantly influenced by many environmental conditions and system configurations, such as soil moisture, soil composition, UG sensor burial depth, AG sink antenna height, and signal operating frequency.

Besides the complex channel characteristics, WUSNs have a heterogeneous network architecture that consists of a large number of UG sensors, fixed AG data sinks and mobile AG data sinks. Such network architecture is necessary due to the challenging channels in WUSNs. Specifically, if there is only one single AG data sink, a prohibitively high density of UG sensors is required to guarantee the full connectivity, due to the small and dynamic transmission range of the UG-UG channel. To solve this problem, multiple AG data sinks are introduced. Since the transmission range of UG-AG channel is much larger than the UG-UG channel, the WUSNs can be connected with much lower UG sensor density. Fixed AG data sinks can be deployed at random positions inside the monitored field, while mobile AG data sinks can be carried by people or machineries inside the monitored field. The mobile sink moves randomly and collects data from the UG sensors when moving into their transmission range. If the WUSN applications can tolerate a certain level of latency, the isolated UG sensors can expect a mobile sink coming and collecting their data. Therefore, the mobile AG sinks can further enhance the network connectivity.

The connectivity analysis in WUSNs is complicated since WUSNs consists of three types of wireless nodes (UG sensors, AG fixed sinks, and mobile sinks) in two different mediums (soil and air) with three different transmission ranges (UG-UG, UG-AG and AG-UG). In addition, the connectivity in WUSNs is highly dynamic due to the dynamic underground channel characteristics and the random movement of the mobile sinks. The tradeoff between the good connectivity and the low latency also needs to be analyzed. Moreover, since the channels between AG and UG devices are asymmetrical, the network connectivity is also asymmetrical. To the best of our knowledge, these problems have not been addressed by the research community so far.

In this paper, we investigate the dynamic connectivity in WUSNs. We develop a mathematical framework to determine the lower and upper bounds of the connectivity probability in WUSNs, which analytically captures the effects of the density and distribution of both the UG sensors and the AG fixed sinks, the number and mobility of the AG mobile sinks, the soil properties especially the dynamic soil moisture, the UG sensor burial depth, the AG sink antenna height, the tolerable latency of the envisioned application, the radio power, and the system operating frequency. Based on the framework, we present numerical and simulation results that quantitatively analyze the effects of various environmental and system parameters on the dynamic connectivity in WUSNs. The results of this paper provide principles and guidelines for the design and deployment of WUSNs to fulfill different application requirements in various environmental conditions.

The remainder of this paper is organized as follows. In Section II, related works are introduced. In Section III, the channel model for WUSNs is presented. In Section IV, the dynamic connectivity problem in WUSNs is mathematically formulated. Next, the lower and the upper bound of the connectivity probability are derived in Section V and Section VI, respectively. Then, in Section VII, simulation studies are performed. Finally, the paper is concluded in Section VIII.

II. Related Work

The connectivity in terrestrial homogenous ad hoc networks has been thoroughly analyzed. In [10], the necessary and sufficient scaling of the transmission range is analyzed to achieve the full connectivity. In [11], the upper bound of the connectivity probability is proposed as a function of the node density. In[12], [13], the network connectivity is investigated in the presence of channel fading and unreliable nodes. In [14], the dynamic connectivity caused by unreliable links is analyzed. All the above works are based on the homogenous networks with only one type of nodes, which is much simpler than the case in WUSNs where three types of wireless devices are deployed in two types of mediums. Moreover the simple terrestrial channel models cannot characterize the complex channels among devices in both underground and aboveground.

The connectivity of terrestrial ad hoc networks with a heterogeneous network architecture is analyzed in [15]. It is proved that the connectivity of ad hoc networks can be improved by deploying base stations under certain conditions. In [16], the connectivity in a sensor network with node sleeping scheme is analyzed. However, the authors assume that only one data sink exists. In [17], multiple sinks are considered in the connectivity analysis in wireless sensor networks. However, the authors assume that sensors can be connected to sinks only in a single-hop fashion. All the above works are based on the determined terrestrial channel model and do not consider the possible connectivity improvement introduced by mobile sinks.

To date, no existing work has addressed the unique connectivity problems in WUSNs as stated in Section I. In this paper, we develop the solutions for these problems.

III. Channel Characteristics in WUSNs

The complex channel characteristics constitute one of the major challenges in the connectivity analysis in WUSNs. We have developed the channel model for UG-UG channel in our previous works [2], [8]. This theoretical model has been validated by the testbed developed in [9]. In this section, we extend this channel model to characterize all the three types of channels in WUSNs, including the UG-UG channel, UG-AG channel, and the AG-UG channel. Moreover, the effects of the lateral waves [18] are considered to improve the model accuracy in the UG-UG channel. It should be noted that the interference problem is assumed to be addressed by a proper MAC protocol for WUSNs in this paper.

A. UG-UG Channel

As shown in Fig. 1(a), three signal paths are considered in the UG-UG channel, including the direct path, the reflected path due to the reflection on the air-ground interface, and the ground surface path due to the lateral waves.

The signal loss of the direct path with length d (meters), $L^d_{UG}(d)$, is given as [2], [8]:

$$L^d_{UG}(d) = 6.4 + 20\log d + 20\log\beta + 8.69\alpha d\ , \tag{1}$$

where α is the attenuation constant with the unit of $1/m$, and β is the phase shifting constant with the unit of $radian/m$. The values of α and β depend on the dielectric properties of soil:

$$\alpha = 2\pi f\sqrt{\frac{\mu\epsilon'}{2}\left[\sqrt{1+(\frac{\epsilon''}{\epsilon'})^2}-1\right]}\ , \qquad \beta = 2\pi f\sqrt{\frac{\mu\epsilon'}{2}\left[\sqrt{1+(\frac{\epsilon''}{\epsilon'})^2}+1\right]}\ , \tag{2}$$

where f is the operating frequency, μ is the magnetic permeability, ϵ' and ϵ'' are functions of the soil properties including soil moisture, bulk density, and soil composition in terms of sand and clay fractions. The detailed expressions of ϵ' and ϵ'' can be found in [2], [8].

Besides the direct path, since the UG sensors may be buried near the air-ground interface (the burial depth is less than 2 m), two more signal paths need to be considered, including 1) the reflected wave on the air-ground interface and 2) the lateral wave traveling along the ground surface, as shown in Fig. 1(a). If the burial depth of the UG sensors is h_u, the total path loss of the UG-UG channel L_{UG-UG} is deduced as:

$$L_{UG-UG} = L^d_{UG}(d) - 10\log V(d, h_u)\ , \tag{3}$$

where $V(d, h_u)$ is the attenuation factor due to the reflected path and the surface path. Because of the different phase shifting, the signals of the reflected path and the surface path may have positive or negative contributions to the signal of the direct path. The influence of the reflected path is analyzed in [2], [8] while the effects of the surface path, i.e. the lateral waves, are discussed in [18]. Hence, by extending the results of the above works, the attenuation factor due to the reflected path and the surface path, $V(d, h_u)$, can be derived by

$$\begin{aligned} V^2(d,h_u) \simeq\, & 1 + \left(G_{rd}\cdot\Gamma\cdot e^{-\alpha\Delta d_1}\right)^2 + 2\cdot G_{rd}\cdot\Gamma\cdot e^{-\alpha\Delta d_1}\cdot\cos\left(\pi-\phi+\beta\Delta d_1\right) \\ & + \left[G_{ld}\cdot e^{-\alpha\Delta d_2}\cdot\overline{E_{d_h}}(d,h_u)\right]^2 + 2\cdot G_{ld}\cdot e^{-\alpha\Delta d_2}\cdot\overline{E_{d_h}}(d,h_u)\cdot\cos\left(\pi+\beta\Delta d_2+k_0 d\right) \\ & + 2\cdot G_{rd}\cdot\Gamma\cdot e^{-\alpha\Delta d_1}\cdot G_{ld}\cdot e^{-\alpha\Delta d_2}\cdot\overline{E_{d_h}}(d,h_u)\cdot\cos\left(\beta\Delta d_2+k_0 d+\phi-\beta\Delta d_1\right), \end{aligned} \tag{4}$$

where Γ and ϕ are the amplitude and phase of the reflection coefficient, $\Delta d_1 = \sqrt{d^2+4h_u^2} - d$ is the length difference of the reflected path and the direct path; $\Delta d_2 = 2h_u - d$ is length difference of the UG part of the lateral wave path and the direct path, as shown in Fig. 1(a); $\overline{E_{d_h}}(d, h_u)$ is the normalized radial component of the electric field caused by the lateral wave when two UG sensors are d meters apart and have a burial depth of h_u meters; the detailed expression of $E_{d_h}(d, h_u)$ is given in [18, equ (5.13)]; k_0 is the wave number of the EM waves in the air; $G_{rd} = e^{(g_t^r + g_r^r - g_t^d - g_r^d)/10}$ and $G_{ld} = e^{(g_t^l + g_r^l - g_t^d - g_r^d)/10}$ are the relative antenna gain factor of the reflected wave and the lateral wave, where g_t^d, g_t^r, and g_t^l are the transmitter antenna gain of the direct wave, reflected wave, and lateral wave, respectively; and g_r^d, g_r^r, and g_r^l are the receiver antenna gain of the direct wave, reflected wave, and lateral wave.

Assuming that the transmit power of the UG sensor is P_t^u, the antenna gains of the receiver and transmitter for the direct path signal are g_r^d and g_t^d. Then the received power, P_r^{U-U}, at a receiver d meters away is $P_r^{U-U} = P_t^u + g_r^d + g_t^d - L_{UG-UG}$. Consequently, the transmission range of the UG-UG channel is:

$$R_{UG-UG} = \max\{d : P_r^{U-U}/P_n > SNR_{th}\}\ , \tag{5}$$

where P_n is the noise power; and SNR_{th} is the required minimum signal-to-noise ratio.

B. UG-AG Channel

Different from the UG-UG channel, the lateral waves have neglectable effects in the UG-AG channel and the AG-UG channel since the path loss of EM waves in the air is much smaller than that of the lateral waves. The reflected path does not exist in the UG-AG channel and the AG-UG channel, either. The path loss of the UG-AG channel L_{UG-AG} consists of three parts: the

UG path loss L_{UG}, the AG path loss L_{AG} and the refraction loss from soil to air L^R_{UG-AG}:

$$L_{UG-AG} = L_{UG}(d_{UG}) + L_{AG}(d_{AG}) + L^R_{UG-AG} \ , \tag{6}$$

where d_{UG} is the length of the UG path, and the d_{AG} is the length of the AG path, as shown in the left of Fig. 1. The UG path loss L_{UG} can be derived from (1). The AG path loss L_{AG} is:

$$L_{AG}(d) = -147.6 + 20 \log d + 20 \log f \ , \tag{7}$$

Since the dielectric constant of soil is much larger than the air, the signals with an incident angle θ_I that is larger than the critical angle θ_c will be completely reflected, where $\theta_c \simeq \arcsin \frac{1}{\sqrt{\epsilon'}}$. Moreover, because the length of the AG path d_{AG} is much larger than the height of the AG sink antenna h_a, the incident angle θ_I is approximately equal to θ_c; and the refracted angle θ_R is approximately equal to $90°$. Then the horizontal distance d between the UG sensor and AG sink is approximately equal to d_{AG}, and $d_{UG} \simeq \frac{h_u}{\cos \theta_c}$. The refraction loss L^R_{UG-AG} can be calculated as:

$$L^R_{UG-AG} \simeq 10 \log \frac{(\sqrt{\epsilon'} + 1)^2}{4\sqrt{\epsilon'}} . \tag{8}$$

Although the the multi-path fading is not significant in most WUSN applications since the WUSNs are mainly deployed in spacious fields (e.g. crop field and playground), we model the AG path as a Rayleigh fading channel to make sure that our analysis is applicable in all possible WUSN scenarios. Specifically, the envelope of the signal of the UG-AG path is modeled as an Rayleigh distributed random variable χ. The probability density function (PDF) of χ is:

$$f(\chi) = \frac{\chi}{\sigma_R^2} e^{-\chi^2/2\sigma_R^2}, \tag{9}$$

where $\sigma_R > 0$ is the Raleigh distribution parameter that can be derived by field experiments in the specific deployed environment.

If the antenna gains of the UG-AG path are g_t and g_r, the received power is $P_r^{U-A} = P_t^u + g_r + g_t - L_{UG-AG} + 10 \log \chi^2$ at the AG sink. Consequently the transmission range of the UG-AG channel is calculated as:

$$R_{UG-AG} \simeq \max\{d_{AG} : P_r^{U-A} / P_n > SNR_{th}\} \ . \tag{10}$$

C. AG-UG Channel

Similar to the UG-AG channel, the path loss of the AG-UG channel is:

$$L_{AG-UG} = L_{UG}(d_{UG}) + L_{AG}(d_{AG}) + L^R_{AG-UG} \ , \tag{11}$$

where L^R_{AG-UG} is the refraction loss from air to soil. As shown in the right of Fig. 1, because the dielectric constant of soil is much larger than the air, most radiation energy from the AG sink will be reflected back if the incident angle θ_I is large. Therefore, we only consider the signal with small incident angle. Consequently, the refracted angle θ_R in the soil is even smaller hence it can be viewed approximately as zero. Then the UG path length $d_{UG} \simeq h_u$; the incident angle $\cos\theta_I = \frac{h_a}{d_{AG}}$; the horizontal distance between the UG sensor and AG sink is $d \simeq \sqrt{d_{AG}^2 - h_a^2}$. Then the refraction loss L_{AG-UG}^R can be calculated as:

$$L_{AG-UG}^R \simeq 10\log\frac{(\cos\theta_I + \sqrt{\epsilon' - \sin^2\theta_I})^2}{4\cos\theta_I\sqrt{\epsilon' - \sin^2\theta_I}} \ . \tag{12}$$

Due to the possible multipath fading in aboveground environments, the AG path in the AG-UG channel is also modeled as a Rayleigh fading channel. Therefore, if the transmit power of the AG sink is P_t^a and the antenna gains of the AG-UG path are g_t and g_r, the received power is $P_r^{A-U} = P_t^a + g_r + g_t - L_{AG-UG} + 10\log\chi^2$ at the UG sensor. Therefore the transmission range of the UG-AG channel is calculated as:

$$R_{AG-UG} \simeq \max\{d : P_r^{A-U}/P_n > SNR_{th}\} \ . \tag{13}$$

D. Numerical Results

The numerical results of the transmission ranges of the channels in WUSNs are shown in Fig. 2 as functions of the volumetric water content (VWC) and the burial depth, where the system and environmental parameters are set as follows. The transmitting power is 10 mW at 900 MHz. The minimum received power for correct demodulation is -90 dBm. The antenna on sensors is ideal dipoles with isotropic radiation pattern. Hence, all paths have the same the antenna gains $g_t = g_r = 5$ dB. The antenna heights of all AG fixed and mobile sinks are 1 m above the ground surface. In the soil medium, the sand particle percent is 50%. The clay percent is 15%. The bulk density is 1.5 grams$/cm^3$, and the solid soil particle density is 2.66 grams$/cm^3$.

Fig. 2 shows that R_{UG-UG} is the smallest while R_{UG-AG} and R_{AG-UG} are much larger. R_{UG-AG} is larger than R_{AG-UG} due to the reflection and refraction on the air-ground interface. Moreover, the soil water content and the sensor burial depth have significant influences on all the three types of channels in WUSNs. Besides, the antenna height of the AG sinks has obvious effect on the AG-UG channel and the multipath fading parameter χ can affect both UG-AG channel and AG-UG channel, the numerical results of which are not given due to the page limit.

According to the channel models provided in this section, in the following sections we denote the transmission range of UG-UG channel R_{UG-UG} as a function of m_v and h_u, i.e. $R_{UG-UG}(m_v, h_u)$; we denote the transmission range of UG-AG channel R_{UG-AG} as a function of

m_v, h_u and χ, i.e. $R_{UG-AG}(m_v, h_u, \chi)$; and we denote the transmission range of AG-UG channel R_{AG-UG} as a function of m_v, h_u, h_a, and χ, i.e. $R_{AG-UG}(m_v, h_u, h_a, \chi)$.

IV. Problem Formulation

After the channel models of the three types of channels in WUSNs are provided, we formulate the problem of the connectivity analysis in WUSNs in this section. We consider a WUSN deployed in a bounded region $\mathbb{R}^2$, as shown in Fig. 3. The UG sensors $\{N_i, i = 1, 2, \cdots\}$ are distributed inside the region $\mathbb{R}^2$ according to a homogeneous Poisson point process of constant spatial intensity λ_u. The AG fixed sinks $\{S_j, j = 1, 2, \cdots\}$ are distributed inside $\mathbb{R}^2$ according to another homogeneous Poisson point process with spatial intensity λ_a. In addition, there are m AG mobile sinks $\{M_k, k = 1, 2, \cdots m\}$ carried by people or machineries inside the region $\mathbb{R}^2$. The monitored region $\mathbb{R}^2$ is much larger than the transmission range of the UG-UG channel. Hence the scale of the network is large and the border effects can be ignored.

A WUSN is defined to be fully connected if every UG sensor is connected to at least one AG data sink in a multi-hop fashion within the tolerable latency. Specifically:

Definition 1: A UG sensor is connected if either of the following statements is true.

- The UG sensor is connected to at least one fixed AG sink directly or in a multi-hop fashion;
- The UG sensor is connected to at least one mobile AG sink directly or in a multi-hop fashion within the duration t_{max}, where t_{max} is the maximum tolerable latency.

Definition 2: A WUSN is fully connected if all its UG sensors are connected.

The functionalities of the WUSNs include two phases: the sensing phase and the control phase. In the sensing phase, the UG sensors report sensing data to the AG sinks, while in the control phase, the AG sinks send control messages to the UG sensors. Since the UG-AG channel and the AG-UG channel are asymmetrical, we analyze the connectivity in the two phases separately. In the sensing phase, the UG-UG and the UG-AG channels are used, while in the control phase UG-UG and the AG-UG channel are utilized. The maximum tolerable latencies in the sensing phase and control phase are t_s and t_c, respectively. $t_s \ll t_c$ in most envisioned applications. Since the only differences between the connectivity analysis in the two phases are the transmission ranges and the tolerable latencies, we calculate the connectivity probability in the sensing phase in the following sections. The connectivity probability in the control phase can be derived from the developed formulas by changing the values of the transmission range and the tolerable latency.

As discussed in Section I, the connectivity in WUSNs is highly dynamic due to the dynamic underground channel characteristics and the random movement of the mobile sinks. Hence, we mathematically formulate these two randomness in the rest part of this section.

A. Randomness Caused by Dynamic Channel Characteristics

The transmission ranges of the three types of channels in WUSNs are functions of soil water content, the sensor burial depth, and sink antenna height. Those parameters are either temporally or spatially random, which cause the randomness of connectivity in WUSNs.

1) Soil Water Content: According to [22] among many other previous works, the daily soil water content data can be well-fitted by a gamma distribution. The gamma distribution can be completely characterized by its mean and variance, which are given by [22]:

$$\mu_{m_v} = \frac{b 2\pi\zeta}{a {r_{_R}}^2 \eta\beta} \ , \qquad \sigma^2_{m_v} = \frac{4\pi\zeta}{\eta\beta^2 {r_{_R}}^2} \frac{b^2}{a(\eta+a)} \ , \tag{14}$$

where ζ is the intensity of the Poisson rain process; a is the normalized soil water loss; b is the rain/irrigation coefficient; $1/r_{_R}$, $1/\eta$, and $1/\beta$ are the mean cell radius, duration, and intensity of each rain, respectively. The probability density function (PDF) of the soil water content is:

$$f(m_v) = m_v^{-1+\mu^2_{m_v}/\sigma^2_{m_v}} \cdot \frac{e^{-m_v \cdot \mu_{m_v}/\sigma^2_{m_v}}}{\left(\frac{\sigma^2_{m_v}}{\mu_{m_v}}\right)^{\mu^2_{m_v}/\sigma^2_{m_v}} \cdot \Gamma(\frac{\mu^2_{m_v}}{\sigma^2_{m_v}})} \ , \tag{15}$$

where $\Gamma(x)$ is the Gamma function [21]; μ_{m_v} and $\sigma^2_{m_v}$ are given in (14). It should be noted that the randomness brought by the dynamic soil water content is only in temporal scale. In a give time stamp, the soil water content throughout the whole field can be considered to be the same.

2) Sensor Burial Depth and Sink Antenna Height: In WUSN applications, the burial depths of all UG sensors are not necessarily the same. Hence, the sensor burial depth throughout the whole WUSN is a random variable. Similarly, the antenna heights of all AG sinks throughout the monitored field are also random variables. We model the random sensor burial depths and sink antenna heights as uniformly distributed variables. Specifically, the UG sensor burial depths are uniformly distributed in $[h_u^{min}, h_u^{max}]$; and the antenna heights of the AG fixed and mobile sinks are uniformly distributed in $[h_a^{min}, h_a^{max}]$. It should be noted that the randomness brought by the different sensor burial depth and the sink antenna height is only in the spatial scale. After the deployment, the burial depth and antenna height remain the same during the WUSN operation.

B. Randomness Caused by AG Sink Mobility

The employment of AG mobile sinks can improve the connectivity in WUSNs but also brings randomness. Since the mobile AG sinks are carried by people or machineries, their movements can be modeled by the widely used Random Waypoint (RWP) Model [19]. In RWP model, the random movement is modeled as a sequence of steps. A step includes a flight and a following pause. In a flight, the sink first select a destination that is uniformly distributed in the whole region $\mathbb{R}^2$. Then the sink starts to move towards the destination with a constant speed v m/s. After it arrives the destination, the sink pauses for τ second and then starts the next step. The speed v and the pause τ are chosen uniformly from $[v_{min}, v_{max}]$ and $[0, \tau_{max}]$, respectively.

V. Lower Bound of Connectivity Probability in WUSNs

The connectivity in WUSNs depends on various environmental and system parameters. Here and in the next section, the lower and upper bounds for the connectivity probability in WUSNs are derived analytically. These theoretical bounds enable the quantitative analysis of the effects of multiple system and environmental parameters on the connectivity in WUSNs.

From Definition 2, the full connectivity probability P_c of WUSNs can be expressed as:

$$P_c = \sum_{n=0}^{\infty} P(\text{All } n \text{ UG sensors are connected}) \cdot P(\text{There are } n \text{ UG sensors in } \mathbb{R}^2) \ . \tag{16}$$

It should be noted that the connectivity probability is zero if there is no sensors in the network. Then in (16), if $n = 0$, we define that $P(0 \text{ UG sensor is connected}) = 0$.

According to the FKG inequality [20] and the homogeneous distribution of the UG sensors,

$$P(\text{All } n \text{ UG sensors are connected}) \geq \prod_{i=1}^{n} P(N_i \text{ is connected}) = P^n(N_i \text{ is connected}) \ . \tag{17}$$

Additionally, since the UG sensors are distributed according to a Poisson point process,

$$P(\text{There are } n \text{ UG sensors in } \mathbb{R}^2) = \frac{(\lambda_u S_{\mathbb{R}^2})^n}{n!} e^{-\lambda_u S_{\mathbb{R}^2}} \ , \tag{18}$$

where $S_{\mathbb{R}^2}$ is the area of the region $\mathbb{R}^2$. Then

$$P_c \geq \sum_{n=0}^{\infty} P^n(N_i \text{ is connected}) \cdot \frac{(\lambda_u S_{\mathbb{R}^2})^n}{n!} e^{-\lambda_u S_{\mathbb{R}^2}} = \exp\Big\{-\lambda_u S_{\mathbb{R}^2} \cdot P(N_i \text{ is not connected})\Big\}. \tag{19}$$

Next, we evaluate the upper bound of $P(N_i$ is not connected) in (19), the probability that a single UG sensor node N_i is not connected. According to Definition 1, we have

$$P(N_i \text{ is not connected}) = P\Big(N_i \not\leftrightarrow \text{fixed sink} \ \cap \ N_i \not\leftrightarrow \text{mobile sink within } t_s\Big) \tag{20}$$

where $A \not\leftrightarrow B$ indicates that A is not connected to B; t_s is the maximum tolerable latency in the sensing phase given in Section IV. Since the event $\{N_i \not\leftrightarrow \text{fixed sink}\}$ and event $\{N_i \not\leftrightarrow \text{mobile sink within } t_s\}$ can be viewed as independent, then

$$P(N_i \text{ is not connected}) = P\Big(N_i \not\leftrightarrow \text{fixed sink}\Big) \cdot P\Big(N_i \not\leftrightarrow \text{mobile sink within } t_s\Big) \tag{21}$$

According to (16) to (21), to derive the lower bound of the connectivity probability P_c, we need to find out the upper bounds of two probabilities, which are the probability that sensor N_i is not connected to all fixed sinks, $P\big(N_i \leftrightarrow\!\!\!\!\times\!\!\!\!\leftrightarrow \text{fixed sink}\big)$, and the probability that sensor N_i is not connected to all mobile sink within time t_s, $P\big(N_i \leftrightarrow\!\!\!\!\times\!\!\!\!\leftrightarrow \text{mobile sink within } t_s\big)$. In the rest part of this section, the upper bounds of the two probabilities are developed.

A. Upper Bound of $P\big(N_i \leftrightarrow\!\!\!\!\times\!\!\!\!\leftrightarrow$ *fixed sink*$\big)$

The probability that the UG sensor N_i is not connected to any fixed AG sinks $P\big(N_i \leftrightarrow\!\!\!\!\times\!\!\!\!\leftrightarrow$ fixed sink$\big)$ can be further developed as

$$P\big(N_i \leftrightarrow\!\!\!\!\times\!\!\!\!\leftrightarrow \text{fixed sinks}\big) \tag{22}$$
$$= \sum_{n=0}^{\infty} P(N_i \leftrightarrow\!\!\!\!\times\!\!\!\!\leftrightarrow S_1 \cap N_i \leftrightarrow\!\!\!\!\times\!\!\!\!\leftrightarrow S_2 \cap \ldots \cap N_i \leftrightarrow\!\!\!\!\times\!\!\!\!\leftrightarrow S_n) \cdot P(\text{There are } n \text{ fixed AG sinks in } \mathbb{R}^2)\ ,$$

where S_j is j^{th} fixed AG sink. Since AG fixed sinks are distributed according to a Poisson point process with density λ_a, $P(\text{There are } n \text{ fixed AG sinks in } \mathbb{R}^2)$ can be calculated using (18) by replacing λ_u with λ_a. $\{N_i \leftrightarrow\!\!\!\!\times\!\!\!\!\leftrightarrow S_{j_1}\}$ and $\{N_i \leftrightarrow\!\!\!\!\times\!\!\!\!\leftrightarrow S_{j_2}\}$ ($j_1 \neq j_2$) are independent events. Then

$$P\big(N_i \leftrightarrow\!\!\!\!\times\!\!\!\!\leftrightarrow \text{fixed sinks}\big) = \sum_{n=0}^{\infty} P^n(N_i \leftrightarrow\!\!\!\!\times\!\!\!\!\leftrightarrow S_j) \cdot \frac{(\lambda_a S_{\mathbb{R}^2})^n}{n!} e^{-\lambda_a S_{\mathbb{R}^2}} = e^{-\lambda_a S_{\mathbb{R}^2} \cdot P(N_i \leftrightarrow S_j)}\ , \tag{23}$$

where $A \leftrightarrow B$ indicates that A is connected to B.

Since the position of the UG sensor N_i and the position of the fixed sink S_j are distributed according to two different homogeneous Poisson point processes, then

$$P\big(N_i \leftrightarrow\!\!\!\!\times\!\!\!\!\leftrightarrow \text{fixed sinks}\big) = \exp\left\{ -\lambda_a S_{\mathbb{R}^2} \cdot \int_{\mathbb{R}^2}\int_{\mathbb{R}^2} \left(\frac{1}{S_{\mathbb{R}^2}}\right)^2 \cdot P\big(\boldsymbol{x}_i \longleftrightarrow \boldsymbol{z}_j\big)\ d\boldsymbol{x}_i d\boldsymbol{z}_i \right\}\ , \tag{24}$$

where $\boldsymbol{x}_i$ is the vector position of sensor N_i; $\boldsymbol{z}_j$ is the vector position of the fixed sink S_j; $P\big(\boldsymbol{x}_i \longleftrightarrow \boldsymbol{z}_j\big)$ is the probability that the UG sensor at $\boldsymbol{x}_i$ is connected to the AG fixed sink at $\boldsymbol{z}_j$.

To derive the lower bound of $P\big(\boldsymbol{x}_i \longleftrightarrow \boldsymbol{z}_j\big)$, we first map the WUSN on a discrete lattice, as shown in Fig. 4. The square lattice L over the region $\mathbb{R}^2$ is constructed as follows. The location of the UG sensor $\boldsymbol{x}_i$ is on one vertex of the lattice, which is set as the origin of the lattice. The straight line ef connecting $\boldsymbol{x}_i$ and $\boldsymbol{z}_j$ forms a sequence of horizontal edges of the lattice L. The length of each edge is d. Let L' be the dual lattice of L. The vertexes of L' are placed in the center of every square of L. The edges of L' crosse every edge of L. According to the above structure, there exists a one-to-one relation between the edges of L and the edges of L'. L and L' have the same edge length $d = \frac{1}{\sqrt{5}} R_{UG-UG}(m_v, h_u^{max})$. The value is chosen so that two UG sensors deployed in two adjacent squares in L' are guaranteed to be connected to each other.

Note that the maximum burial depth h_u^{max} is used here to achieve the lower bound of the UG-UG communication range. Moreover, the soil water content m_v is a random variable as discussed in Section IV, and $R_{UG-UG}(m_v, h_u^{max})$ is a function of the soil water content m_v. Hence the edge length of the lattice d is also a random variable. Note that all the edges in L and L' have the same length $d(m_v)$ at one time stamp while $d(m_v)$ is random in different time stamps. Some definitions are first given:

Definition 3: An edge l' in L' is said to be open if both squares adjacent to l contains at least one UG sensor.

Definition 4: An edge l of the L is said to be open if the corresponding edge of L' is open.

Definition 5: A path of the L or $L's$ is said to be open (closed) if all edges forming the path are open (closed).

Now consider the connection between the sensor at $\boldsymbol{x}_i$ and the sink at $\boldsymbol{z}_j$. The region $\mathbb{R}^2$ is divided into two parts, the region inside the circle $C_{\boldsymbol{z}_j}$ and the region outside the circle. $C_{\boldsymbol{z}_j}$ is defined as the circle with radius $R_{UG-AG}(m_v, h_u^{max}, \chi)$ and center located at $\boldsymbol{z}_j$, as shown in Fig. 4. Again, the maximum burial depth h_u^{max} is used here to achieve the lower bound of the UG-AG channel range. Then the UG-AG channel range $R_{UG-AG}(m_v, h_u^{max}, \chi)$ is a function determined by two random variables: the soil water content m_v and the multipath fading parameter χ. The UG-AG channel range R_{UG-AG} is used here since we aim to calculate the connectivity probability in sensing phase of the WUSNs. For the control phase of the WUSNs, the UG-AG channel range R_{AG-UG} is used and the connectivity probability of the control phase can be derived in the similar way.

If there is an open path of L connecting $\boldsymbol{x}_i$ and a vertex V of L inside $C_{\boldsymbol{z}_j}$, then UG sensor and the AG sink are guaranteed to be connected by each other. Note that the square in L' containing vertex V should be completely inside the circle $C_{\boldsymbol{z}_j}$. The set of these open paths is denoted as $\boldsymbol{P}_o = \{P_o^1, P_o^2, ...\}$, where $P_o^1, P_o^2, ...$ denote all possible open paths. Then,

$$P\left(\boldsymbol{x}_i \leftrightarrow \boldsymbol{z}_j \middle| m_v, \chi\right) \geq P\left(\cup_i^\infty P_o^i\right) , \tag{25}$$

where $P\left(\boldsymbol{x}_i \leftrightarrow \boldsymbol{z}_j \middle| m_v, \chi\right)$ is the conditional probability assuming that m_v and χ are given. Due to the randomness of the positions of the UG sensors and AG sinks, it is impossible to derive the exact expression of $P\left(\cup_i^\infty P_o^i\right)$. Hence, we use two methods to calculate the lower bound of this probability:

- When the UG sensor density is high, we use the maximum probability that a certain open path exists, i.e. $\max_i\{P(P_o^i)\}$, as the lower bound of $P\left(\cup_i^\infty P_o^i\right)$ since $P\left(\cup_i^\infty P_o^i\right) > P(P_o^i)$, where $i = 1, 2, ...\infty$.

- When the UG sensor density is low, we calculate the lower bound of the probability that there is at least one open path, i.e. $P\big(|\boldsymbol{P}_o| > 0\big)$, as the lower bound of $P\big(\cup_i^\infty P_o^i\big)$ since $P\big(\cup_i^\infty P_o^i\big) = P\big(|\boldsymbol{P}_o| > 0\big)$. Note that $|\boldsymbol{P}_o|$ is the number of the existing open paths and $P\big(|\boldsymbol{P}_o|>0\big) = 1-P\big(|\boldsymbol{P}_o|=0\big)$.

The above two bounds are both valid lower bound of $P\big(\cup_i^\infty P_o^i\big)$. We use the larger one of the two bounds in our analysis, which depends on the UG sensor density. Therefore,

$$P\big(\boldsymbol{x}_i \leftrightarrow \boldsymbol{z}_j \big| m_v, \chi\big) \geq \max\left\{ \max_i\{P(P_o^i)\},\ 1-P\big(|\boldsymbol{P}_o|=0\big)\right\}. \tag{26}$$

We first calculate $\max_i\{P(P_o^i)\}$ in (26). Since the UG sensors are distributed according to a homogeneous Poisson point process, the shortest open path connecting $\boldsymbol{x}_i$ and $\boldsymbol{z}_j$ can yield the maximum existing probability. Specifically, the shortest path is the line segment on ef between $\boldsymbol{x}_i$ and the first vertex of L inside C_{z_j}. This line segment is illustrated by the thick gray segment in Fig. 4. The length of the line segment is Wd, where

$$W = \begin{cases} \left\lceil \frac{||\boldsymbol{x}_i - \boldsymbol{z}_j|| - R_{UG-AG}(m_v, h_u)}{d} \right\rceil + 1, & \text{if } ||\boldsymbol{x}_i - \boldsymbol{z}_j|| \geq R_{UG-AG}(m_v, h_u^{max}, \chi) \\ 0, & \text{if } ||\boldsymbol{x}_i - \boldsymbol{z}_j|| < R_{UG-AG}(m_v, h_u^{max}, \chi) \end{cases} \tag{27}$$

where $\lceil a \rceil$ means rounding a to the nearest integer $\geq a$. Hence,

$$\begin{aligned} \max_i\{P(P_o^i)\} &= P(\text{There exists an open path with length } W) \\ &= P^{W+1}(\text{There exists at least one sensor in a square } d^2) = (1-q)^{W+1}, \end{aligned} \tag{28}$$

where

$$q = P(\text{There is no sensor in a square } d^2) = e^{-\lambda_u d^2}. \tag{29}$$

We then calculate $P\big(|\boldsymbol{P}_o|=0\big)$ in (26). The event $\big|\{P_o\}\big| = 0$ indicate that there is no open path connecting the UG sensor at $\boldsymbol{x}_i$ and another UG sensor inside the circle C_{z_j}. Hence, $\big|\{P_o\}\big| = 0$ if and only if the sensor $\boldsymbol{x}_i$ is enclosed by at least one closed circuit of the dual lattice L'. The overlapped area of the closed circuit and the circle C_{z_j} should not contain a whole square of the dual lattice L'. C_1 and C_2 (thick black circuits) in Fig. 4 are examples of such closed circuits. Hence, $P\big(|\boldsymbol{P}_o|=0\big)$ can be evaluated by counting the number of such closed circuits in L'. Let $\rho(n)$ be the number of circuits in L' which have length nd and contain $\boldsymbol{x}_i$ in their interiors. To contain $\boldsymbol{x}_i$ in their interiors, those circuits pass through some point on the line ef, as shown in Fig. 4. The position of the corresponding pass vertex in L' has the form of $(kd - \frac{1}{2}d, \frac{1}{2}d)$. k cannot be larger than $\lfloor \frac{n}{2} \rfloor - 1$. Otherwise the circuits would have a length larger than n. Thus, such a circuit contains a self-avoiding walk of length $n-1$ starting from a vertex at $(kd-\frac{1}{2}d, \frac{1}{2}d)$ and $k > \lfloor \frac{n}{2} \rfloor - 1$. Moreover, to contain $\boldsymbol{x}_i$ inside, the length of the circuits $n \geq 4$. The number of self avoiding walks of L' having length n and beginning at a vertex is denoted as $\sigma(n)$. It has been proven in [20] that $\sigma(n) \leq 4 \cdot 3^{n-1}$ in a 2-D plane.

Since those closed circuits do not contain a whole common square with the circle C_{z_j}, such as C_1 or C_2 in Fig. 4, they must pass through at least one point on the shortest path connecting $\boldsymbol{x}_i$ and $\boldsymbol{z}_j$ (illustrated by the thick gray segment in Fig. 4). Hence, those closed circuits contain a self-avoiding walk of length $n-1$ $(n \geq 4)$ starting from a vertex at $(kd - \frac{1}{2}d, \frac{1}{2}d)$ and $k \leq \min\{\lfloor \frac{n}{2} \rfloor - 1, W\}$. The total number of such closed circuits is denoted as CN. Based on the above discussions, the upper bound of CN can be calculated as follows.

$$CN \leq \sum_{n=4}^{\infty} \sigma(n-1) + \sum_{n=6}^{\infty} \sigma(n-1) + \cdots \sum_{n=2W}^{\infty} \sigma(n-1) \ . \tag{30}$$

Then the upper bound of $P\big(|\boldsymbol{P}_o|=0\big)$, the probability that there is no open path connecting the UG sensor at $\boldsymbol{x}_i$ and the AG fixed sink at $\boldsymbol{z}_j$, is:

$$P\big(|\boldsymbol{P}_o|=0\big) \leq \sum_{i=2}^{W} \sum_{n=2i}^{\infty} \sigma(n-1) \cdot q^n = \begin{cases} 36 \cdot q^4 \cdot \frac{1-(3q)^{2W-2}}{(1+3q)(1-3q)^2} \ , & \text{if } q < \frac{1}{3} \\ 1 \ , & \text{if } q \geq \frac{1}{3} \end{cases} \tag{31}$$

Substituting (28) and (31) into (26), we derive

$$P\big(\boldsymbol{x}_i \leftrightarrow \boldsymbol{z}_j \big| m_v, \chi\big) \geq \begin{cases} \max\left\{(1-q)^{W+1},\ 1-\frac{36q^4[1-(3q)^{2W-2}]}{(1+3q)(1-3q)^2}\right\}, & \text{if } q < \frac{1}{3} \\ (1-q)^{W+1}, & \text{if } q \geq \frac{1}{3} \end{cases} \tag{32}$$
$$\stackrel{\text{def}}{=} \gamma_1(\boldsymbol{x}_i, \boldsymbol{z}_j, \lambda_u, m_v, h_u) \ .$$

According to Section III and IV, the probability without conditions $P\big(\boldsymbol{x}_i \leftrightarrow \boldsymbol{z}_j\big)$ is given by:

$$P\big(\boldsymbol{x}_i \leftrightarrow \boldsymbol{z}_j\big) = \iint P\big(\boldsymbol{x}_i \leftrightarrow \boldsymbol{z}_j \big| m_v, h_u\big) \cdot f(m_v) \cdot f(\chi)\, dm_v d\chi, \tag{33}$$

where $f(m_v)$ and $f(\chi)$ are the PDF of the soil water content given in (15) and the PDF of the multipath fading parameter given in (9), respectively. Substituting (32) and (33) into (24) yields the upper bound of $P\big(N_i \nleftrightarrow \text{fixed sink}\big)$:

$$P\big(N_i \nleftrightarrow \text{fixed sink}\big) \leq \exp\left\{-\frac{\lambda_a}{S_{\mathbb{R}^2}} \iiiint f(m_v) \cdot f(\chi) \cdot \gamma_1(\boldsymbol{x}_i, \boldsymbol{z}_j, \lambda_u, m_v, h_u) d\boldsymbol{x}_i d\boldsymbol{z}_i dm_v d\chi\right\}. \tag{34}$$

B. Upper Bound of $P\big(N_i \nleftrightarrow$ mobile sink within $t_s\big)$

Beside fixed sinks, mobile sinks also contribute to the connectivity in WUSNs. In this sub-section, we calculate the upper bound of the probability that a UG sensor N_i is not connected to any mobile sink within time t_s, i.e. $P\big(N_i \leftrightarrow\!\!\!\!\times\!\!\!\!\leftrightarrow \text{ mobile sink within } t_s\big)$ in (21). Due to the sink mobility, the contributions of the multi-hop connection is much smaller than the direct connection. Hence, only the direct connection is considered while deriving the upper bound, i.e.

$$P\big(N_i \leftrightarrow\!\!\!\!\times\!\!\!\!\leftrightarrow \text{mobile sink within } t_s\big) \leq P\big(N_i \overset{\text{direct}}{\leftrightarrow\!\!\!\!\times\!\!\!\!\leftrightarrow} \text{ mobile sink within } t_s\big) \,. \tag{35}$$

As discussed previously, m mobile sinks move in region $\mathbb{R}^2$ according to RWP model. The stationary node distribution of RWP model is provided in [23], while the intermeeting time between the mobile nodes in RWP model is proved to be exponentially distributed in [24]. We utilize their results to derive the upper bound of $P\big(N_i \overset{\text{direct}}{\leftrightarrow\!\!\!\!\times\!\!\!\!\leftrightarrow} \text{ mobile sink within } t_s\big)$. The sensor N_i is regarded as directly connected by the mobile sinks if at least one of the m mobile sinks visits the UG-AG range around N_i at least once during the time slot $[0, t_s]$. Let $H_k(t)$ be the event that the k^{th} mobile sink does not directly cover the sensor N_i at time stamp t, then

$$P\big(N_i \overset{\text{direct}}{\leftrightarrow\!\!\!\!\times\!\!\!\!\leftrightarrow} \text{ mobile sink within } t_s\big) = P\Big(\cap_{t\in[0,t_s]} \cap_{k=1,\dots,m} H_k(t)\Big), \tag{36}$$

Note that the event $H_k(t)$ is determined by the position of the sensor N_i and the k^{th} mobile sink, the soil water content, and the sensor burial depth. Let $\boldsymbol{y}_k(t)$ denotes the position of the k^{th} sink at time stamp t. Similar to the previous analysis, the maximum burial depth h_u^{max} is used here to achieve the lower bound of the UG-AG channel range. Then, if sensor node N_i's position $\boldsymbol{x}_i$, the soil water content m_v, and the multipath fading parameter χ are given, the event $H_k(t)$ can be further expressed as

$$\{H_k(t)\big|\boldsymbol{x}_i, m_v, \chi\} = \{||\boldsymbol{y}_k(t) - \boldsymbol{x}_i|| > R_{UG-AG}(m_v, h_u^{max}, \chi)\}, \tag{37}$$

where $R_{UG-AG}(m_v, h_u^{max}, \chi)$ is the communication range of the UG-AG channel given in Section III. Then the probability that event $\big\{\cap_{k=1,\dots,m}\ H_k(t)\big\}$ in (36) happens is

$$P\Big(\cap_{k=1,\dots,m}\ H_k(t)\Big) = \frac{1}{S_{\mathbb{R}^2}} \iiint P\Big(\cap_{k=1\dots m} H_k(t)\big|\boldsymbol{x}_i, m_v, \chi\Big) \cdot f(m_v) \cdot f(\chi)\, d\boldsymbol{x}_i dm_v d\chi, \tag{38}$$

where the conditional probability $P\Big(\cap_{k=1,\dots,m}\ H_k(t)\big|\boldsymbol{x}_i, m_v, \chi\Big)$ can be calculated by

$$P\Big(\cap_{k=1,\dots,m}\ H_k(t)\big|\boldsymbol{x}_i, m_v, \chi\Big) = \left(\int_{\boldsymbol{x}\in \mathbb{R}^2 - \mathbb{C}^2[\boldsymbol{x}_i,\, R_{UG-AG}(m_v, h_u^{max}, \chi)]} \xi(\boldsymbol{x})\ d\boldsymbol{x}\right)^m \overset{\text{def}}{=} \gamma_2^m(\boldsymbol{x}_i, m_v, \chi), \tag{39}$$

where $\mathbb{C}^2[\boldsymbol{x}_i, R_{UG-AG}(m_v, h_u^{max}, \chi)]$ is the disk region centered at $\boldsymbol{x}_i$ with radius $R_{UG-AG}(m_v, h_u^{max}, \chi)$; $\xi(\boldsymbol{x})$ is the PDF that a sink visit the position $\boldsymbol{x}$ at arbitrary time stamp (stationary node distribution), which is defined by the RWP model; the detailed expression of $\xi(\boldsymbol{x})$ is given in [23].

Denote the maximum flight length as D in the convex region $\mathbb{R}^2$. Then the maximum time duration t_D for a sink to finish two sequential flights is $t_D = 2(\tau_{max} + D/v_{min})$, where τ_{max}

and v_{min} are the maximum pause time and the minimum velocity of each flight, respectively.

The current positions of all the sinks are independent with their positions t_D ago since all the sinks have already finished at least two flights. We choose an index set of time stamps in $[0,\, t_s]$, i.e. $\boldsymbol{T}_D = \left\{0,\, t_D,\, 2t_D, ...,\, \lfloor \frac{t_s}{t_D} \rfloor \cdot t_D \right\}$. Then the events $\{\cap_{k=1,...,m} H_k(t_j), t_j \in \boldsymbol{T}_D\}$ are all independent. Hence,

$$P\Big(\cap_{t\in[0,t_s]}\cap_{k=1,...,m}H_k(t)\Big) \leq P\Big(\cap_{t_j\in\boldsymbol{T}_D}\cap_{k=1,...,m}H_k(t_j)\Big) = P^{\lfloor t_s/t_D \rfloor}\Big(\cap_{k=1,...,m}\; H_k(t)\Big)\;, \quad (40)$$

Substituting (36)-(40) into (35) yields the upper bound of $P\big(N_i \nleftrightarrow \text{mobile sink within } t_s\big)$:

$$P\big(N_i \nleftrightarrow \text{mobile sink within } t_s\big) \leq \left(\frac{1}{S_{\mathbb{R}^2}} \cdot \iiint \gamma_2^m(\boldsymbol{x}_i, m_v, \chi) \cdot f(m_v) \cdot f(\chi)\; d\boldsymbol{x}_i dm_v d\chi\right)^{\lfloor \frac{t_s}{t_D} \rfloor}. \quad (41)$$

C. Lower Bound of the Connectivity Probability in WUSNs

According to the above analysis, the lower bound of the connectivity probability in WUSNs can be derived by substituting (21) into (19):

$$P_c \geq \exp\Big[-\lambda_u \cdot S_{\mathbb{R}^2} \cdot P\big(N_i \nleftrightarrow \text{fixed sink}\big) \cdot P\big(N_i \nleftrightarrow \text{mobile sink within } t_s\big)\Big]. \quad (42)$$

where $P\big(N_i \nleftrightarrow \text{mobile sink within } t_s\big)$ is given by (41); and $P\big(N_i \nleftrightarrow \text{fixed sink}\big)$ is given by (34).

VI. Upper Bound of Connectivity Probability in WUSNs

The absence of isolated UG sensor is a necessary but not sufficient condition for the full connectivity in WUSNs. Hence the probability that there are no isolated UG sensors is an upper bound for the connectivity probability in WUSNs. Therefore,

$$\begin{aligned} P_c &\leq P(\text{no isolated UG sensor}) \quad (43)\\ &= \sum_{n=0}^{\infty} P(\text{All } n \text{ UG sensors are not isolated}) \cdot P(\text{There are } n \text{ UG sensors in } \mathbb{R}^2). \end{aligned}$$

The isolation events of each node can be viewed as independent according to [11]. Hence

$$P(\text{no isolated UG sensor}) = \sum_{n=0}^{\infty} P^n(N_i \text{ is not isolated}) \cdot P(\text{There are } n \text{ sensors in } \mathbb{R}^2). \quad (44)$$

Then using the same strategy in (18) and (19), we derive:

$$P_c \leq \exp\Big\{-\lambda_u\, S_{\mathbb{R}^2} \cdot P(N_i \text{ is isolated})\Big\}\,. \quad (45)$$

To derive the upper bound of P_c in (45), we analyze the lower bound of the probability $P(N_i$ is isolated). If the soil water content m_v and the multipath fading parameter χ are given,

$P(N_i$ is isolated) can be calculated by utilizing the conditional probability, i.e.

$$P(N_i \text{ is isolated}) = \iint P(N_i \text{ is isolated}\big|m_v, \chi)\cdot f(m_v)\cdot f(\chi)\, dm_v d\chi, \; . \tag{46}$$

Moreover, a UG sensor is isolated, if and only if no other UG sensors, AG fixed sinks and AG mobile sinks exist inside its transmission range. Hence,

$$\begin{aligned} P(N_i \text{ is isolated}\big|m_v, \chi) &= P(\text{no sensor, fixed sink, mobile sink in } N_i\text{'s range}\big|m_v, \chi) \\ &= P(\text{no other UG sensor in } N_i\text{'s range}\big|m_v) \cdot P(\text{no fixed sink in } N_i\text{'s range}\big|m_v, \chi) \\ &\quad \cdot P(\text{no mobi. sink moves in } N_i\text{'s range within } t_s\big|m_v, \chi)\, . \end{aligned} \tag{47}$$

Since UG sensors are distributed according to a Poisson point process with density λ_u,

$$\begin{aligned} &P(\text{no other UG sensor in } N_i\text{'s range}\big|m_v) \\ &\quad = P(N_i \text{ has no sensor neighbor}\big|m_v) \geq e^{-\lambda_u \pi R^2_{UG-UG}(m_v, h_u^{min})}\, . \end{aligned} \tag{48}$$

Note that the minimum burial depth h_u^{min} is used here to achieve the upper bound of the UG-AG channel range.

Similarly, AG fixed sinks are distributed according to a Poisson point process with density λ_a.

$$P(\text{no fixed sink in } N_i\text{'s range}\big|m_v, \chi) \geq e^{-\lambda_a \pi R^2_{UG-AG}(m_v, h_u^{min}, \chi)}\, . \tag{49}$$

The probability that a UG sensor is connected to a mobile sink is affected by the position of the UG sensor. Hence,

$$\begin{aligned} &P(\text{no mobi. sink moves in } N_i\text{'s range within } t_s\big|m_v, \chi) \\ &= \frac{1}{S_{\mathbb{R}^2}} \int_{S_{\mathbb{R}^2}} P(\text{no mobi. sink in } \boldsymbol{x}_i\text{'s range within } t_s\big|m_v, \chi)\; d\boldsymbol{x}_i \\ &= \frac{1}{S_{\mathbb{R}^2}} \int_{S_{\mathbb{R}^2}} \Big[1 - P(k^{th} \text{ mobi. sink is in } \boldsymbol{x}_i\text{'s range within } t_s\big|m_v, \chi)\Big]^m d\boldsymbol{x}_i . \end{aligned} \tag{50}$$

Since the mobile sinks have limited moving velocity, i.e. $v < v_{max}$, the upper bound of the probability $P(k^{th}$ mobi. sink is in $\boldsymbol{x}_i$'s range within $t_s\big|m_v, \chi)$ can be derived by assuming that the mobile sink moves towards $\boldsymbol{x}_i$ with its maximum velocity at the time stamp 0. Therefore,

$$\begin{aligned} P(k^{th} \text{ mobi. sink is in } \boldsymbol{x}_i\text{'s range within } t_s\big|m_v, \chi) &\leq \int_{\boldsymbol{x} \in \mathbb{C}^2[\boldsymbol{x}_i,\, R_{UG-AG}(m_v, h_u^{min}, \chi) + v_{max}\cdot t_s]} \xi(\boldsymbol{x})\; d\boldsymbol{x} \\ &\overset{\text{def}}{=} \gamma_3(\boldsymbol{x}_i, m_v, \chi)\;, \end{aligned} \tag{51}$$

where $\mathbb{C}^2[\boldsymbol{x}_i,\, R_{UG-AG}(m_v, h_u^{min}, \chi) + v_{max}\cdot t_s]$ is the circular region centered at $\boldsymbol{x}_i$ with radius $R_{UG-AG}(m_v, h_u^{min}, \chi) + v_{max}\cdot t_s$; $\xi(\boldsymbol{x})$ is the PDF of the stationary node distribution in the RWP model, which is given in [23]. By substituting (46)-(51) into (45), the upper bound of the connectivity probability in WUSNs is obtained.

$$P_c \leq \exp\Bigg\{ -\lambda_u \int_{m_v} \int_{\chi} \int_{\boldsymbol{x}_i} e^{-\pi \left[\lambda_u \cdot R^2_{UG-UG}(m_v, h_u^{min}) + \lambda_a \cdot R^2_{UG-AG}(m_v, h_u^{min}, \chi)\right]} \cdot \Big[1 - \gamma_3(\boldsymbol{x}_i, m_v, \chi)\Big]^m \cdot f(m_v)\ dm_v\, d\chi\, d\boldsymbol{x}_i \Bigg\}. \tag{52}$$

VII. Performance Evaluation

According to the analytical results shown in (42) and (52), the lower and upper bounds of the connectivity probability in WUSNs are functions of multiple system and environmental parameters, including the UG sensor node density λ_u, the AG fixed sink density λ_a, the number of AG mobile sinks m, the mobility model of the mobile sinks, the tolerable latency (t_s in the sensing phase and t_c in the control phase), the transmission ranges (R_{UG-UG}, R_{UG-AG} in sensing phase and R_{UG-UG}, R_{AG-UG} in control phase), the operating frequency, the distribution of the random soil water content, the sensor burial depth, and the sink antenna height. In this section, we numerically analyze the effects of the above system and environmental parameters on the connectivity in WUSNs. The theoretical probability bounds are validated by the simulations in the meantime. Note that the analysis is based on the sensing phase unless otherwise specified.

Except studying the effects of certain parameters, the default values are set as follows: The monitored region is a $500\ m \times 500\ m$ square. The UG sensors are deployed according to a homogeneous Poisson point process of spatial intensity λ_u with random burial depths. The density of the UG sensor node λ_u is in the range from $0.05\ m^{-2}$ to $1.6\ m^{-2}$. The mean number of the UG sensor node is calculated by multiplying the region area by the UG sensor node density λ_u. The burial depths of all the UG sensors are uniformly distributed in the interval $[0.4, 0.6]$ m (i.e. the mean burial depth is 0.5 m). The density of the fixed AG sinks λ_a is $0.001 m^{-2}$. There are 10 mobile AG sinks moving inside the region according to RWP model. The velocity of each flight is uniformly chosen from $[1, 2]$ m/s. The pause duration is uniformly chosen from $[0, 30]$ sec. The tolerable latencies are $t_s = t_c = 30$ sec in both the sensing phase and the control phase. All the transceivers in sensors and sinks are assumed to be the same. The transmitting power is 10 mW at 900 MHz. The minimum received power for correct demodulation is -90 dBm. The antenna on sensors is ideal dipoles with isotropic radiation pattern. Hence, the antenna has the same gain for all paths from different directions, i.e. $g_t = g_r = 5$ dB. The antenna heights of all AG fixed and mobile sinks are uniformly distributed in the interval $[0.8, 1.2]$ m (i.e. the mean antenna height is 1 m). The Rayleigh distribution parameter of χ in the multipath fading aboveground environment is $\sigma_R = \sqrt{\frac{2}{\pi}}$. In the soil medium, the sand particle percent is 50%. The clay percent is 15%. The bulk density is 1.5 grams/cm^3, and the solid soil particle density is 2.66 grams/cm^3. The volumetric water content (VWC) in the soil is randomly distributed according to a gamma distribution defined in (15), where the mean is $\mu_{m_v} = 8\%$ and the variance $\sigma_{m_v}^2 = 10^{-4}$.

In Fig. 5 to Fig. 11, the theoretical upper and lower bounds are compared with the simulation results with various system and environmental parameters. Each simulated connectivity probability is calculated based on 500 simulation iterations. The lower and upper bounds are calculated by (42) and (52) respectively. As shown in Fig. 5 to Fig. 11, the theoretical upper and lower bounds are valid in all the simulation scenarios. It should be noted that the upper bound is tighter than the lower bound, since the sufficient condition of the connectivity (lower bound) is more difficult to achieve than the necessary condition (upper bound).

Fig. 5 shows the upper bound, lower bound, and the simulation results of the connectivity in a WUSN with the default parameters. The connectivity probability increases as the UG sensor density increases. There exists a turning point in x-axis, where the WUSN has a high probability to be fully connected if the UG sensor density is larger than the turning point. This result is consistent with the connectivity analysis of terrestrial wireless networks. In the following part of this section, the unique effects of various parameters of the WUSN system and the underground environments on the WUSN connectivity are discussed.

A. Soil Moisture

The effects of the higher soil moisture on the WUSNs' connectivity are illustrated in Fig. 6, where the connectivity probabilities are given as a function of UG sensor node density in soil medium with much higher soil moisture. Instead of the 8% mean VWC in default settings, the mean VWC in Fig. 6 is 22%. The variance $\sigma_{m_v}^2$ remains the same. It indicates that the connectivity in WUSNs highly depends on the soil moisture. To achieve equal connectivity probability, the UG sensor node density of the WUSN in wet soil ($\mu_{m_v} = 22\%$) is more than twice of the density required in dry soil ($\mu_{m_v} = 8\%$). This is because the transmission ranges of both the UG-UG and the UG-AG channel are significantly reduced when the water content in the soil increases.

B. Sensor Burial Depth

In Fig. 7, the effects of the deeper sensor burial depth on the WUSNs' connectivity are captured, where the mean sensor burial depth is doubled, i.e. the burial depth is uniformly distributed in the interval $[0.8, 1.2]$ m. Similar to the influence of the soil moisture, the connectivity probability in WUSNs dramatically decreases if the sensor burial depth increases, since the transmission range of the UG-AG channel significantly decreases as sensor burial depth increases. Note that the impacts of the sensor burial depth are smaller that the impacts of the soil moisture, since the burial depth does not dramatically affect the UG-UG channel while the soil moisture influence both the UG-UG channel and the UG-AG channel.

C. Number of Mobile Sinks and Fixed Sink Density

In Fig. 8 and Fig. 9, the effects of mobile sink number and fixed sink density on the connectivity in WUSNs are investigated. Specifically, in Fig. 8, four times more AG mobile sinks are added ($m = 50$), while in Fig. 9, the density of the AG fixed sinks is doubled ($\lambda_a = 0.002\ m^{-2}$) compared with the default parameters. It is shown that the connectivity probabilities increase if the number of mobile sinks or the fixed sink density increases, which can be explained by the definition of WUSN connectivity. With larger fixed sink density, both upper and lower bound of the connectivity probability dramatically increase. However, the lower bound of connectivity probability does not significantly increase with more mobile sinks. Due to the highly random mobility of the mobile sinks, the sufficient conditions (lower bound) are not becoming significantly easier to achieve with more mobile sinks.

D. Tolerable Latency and Sink Mobility

Fig. 10 shows the effect of the longer tolerable latency on the network connectivity, where the tolerable latency is prolonged from 30 sec to 300 sec. As expected, the connectivity probability increases with longer tolerable latency. Therefore, there exists a tradeoff between the lower latency and higher connectivity probability. In Fig. 10, with the 300 sec tolerable latency, the upper bound of the WUSN connectivity probability become constant 100% since the mobile sink can move to any position in the monitored region within the prolonged tolerable latency in the best case. However, similar to the effects of the mobile sink number, the tolerable latency does not have obvious effects on the lower bound of the WUSN connectivity due to the highly random mobility model. It should be noted that the effects of the mobility model parameters (moving velocity and pause time), are similar to the tolerable latency, since the tolerable latency and mobility model parameters have equal effects in determining whether the mobile sink can move into the range of a UG sensor or not.

E. Connectivity in Control Phase

Due to the asymmetrical channel between the UG sensors and AG sinks, the connectivity performances of the sensing phase and the control phase are different. In Fig. 11, the connectivity probability of a WUSN with the default parameters in the control phase is shown as a function of the UG sensor density. Compared with the sensing phase, the connectivity probability in the control phase is obviously lower due to the following reason. In the control phase, the AG-UG channel is utilized. Since the transmission range of the AG-UG channel is much smaller than the UG-AG channel as discussed in Section III, the coverages of either the fixed sinks or the mobile sinks in the control phase are much smaller. Consequently, the connectivity probability decreases in the control phase. The effects of all the system and environmental parameters on the WUSN connectivity in sensing phase are similar in control phase. Besides, the antenna height of the AG fixed and mobile sinks may influence the connectivity in WUSNs since the AG-UG channel is affected by the AG sink antenna heights.However, the influence of the antenna heights is not as significant as the influence of the sensor burial depth since the path loss in the soil is much larger than the path loss in the air.

VIII. Conclusions

The soil medium and the heterogeneous network architecture make the WUSN connectivity analysis much more complex than the terrestrial wireless sensor networks. On the one hand, the WUSNs consist of three types of wireless nodes (UG sensors, AG fixed sinks, and AG mobile sinks) in two different media (soil and air) with three different types of channels (UG-UG, UG-AG and AG-UG). On the other hand, all the three types of channels in WUSNs have completely different characteristics from the terrestrial channels and are significantly affected by multiple underground environmental conditions. In this paper, the dynamic network connectivity in WUSNs is theoretically investigated. The upper and lower bounds of the connectivity probability are analytically developed to provide the necessary and sufficient conditions to achieve the full-connected network, which give the guidelines to design the system parameters of the WUSNs according to the environmental conditions. The analysis results quantitatively capture the effects of multiple system and environmental parameters on the WUSN connectivity, including the UG sensor density, the AG fixed sink density, the number of AG mobile sinks, the UG sensor burial depth, the AG sink antenna height, the soil moisture, the tolerable latency, and the mobility of the AG mobile sinks.

Acknowledgment

This work is based upon work supported by the US National Science Foundation (NSF) under Grant No. CCF-0728889.

REFERENCES

[1] I. F. Akyildiz and E. P. Stuntebeck, “Wireless underground sensor networks: Research challenges,” *Ad Hoc Networks Journal (Elsevier)*, vol. 4, pp. 669-686, July 2006.

[2] I. F. Akyildiz, Z. Sun and M. C. Vuran, “Signal Propagation Techniques for Wireless Underground Communication Networks,” *Physical Communication Journal (Elsevier)*, Vol. 2, No. 3, pp.167-183, September 2009.

[3] Z. Sun and I. F. Akyildiz, “Connectivity in Wireless Underground Sensor Networks,” in *Proc. IEEE SECON ’10*, Boston, MA, USA, June 2010.

[4] Z. Sun, et.al., “BorderSense: Border Patrol through Advanced Wireless Sensor Networks,” in *Ad Hoc Networks Journal (Elsevier)*, vol. 9, no. 3, pp. 468-477, May, 2011.

[5] Z. Sun, et.al., “MISE-PIPE: Magnetic Induction-based Wireless Sensor Networks for Underground Pipeline Monitoring,” in *Ad Hoc Networks Journal (Elsevier)*, vol. 9, no. 3, pp. 218-227, May, 2011.

[6] H. R. Bogena, J. A. Huisman, H. Meier, U. Rosenbaum, and A. Weuthen, “Hybrid Wireless Underground Sensor Networks: Quantification of Signal Attenuation in Soil,” *Vadose Zone J.*, vol. 8, no. 3, pp. 755-761, August 2009.

[7] J. Tiusanen, “Wireless Soil Scout Prototype Radio Signal Reception Compared to the Attenuation Model,” *Precision Agriculture*, DOI 10.1007/s11119-008-9096-7, November 2008.

[8] L. Li, M. C. Vuran, and I. F. Akyildiz, “Characteristics of Underground Channel for Wireless Underground Sensor Networks,” in *Proc. IFIP Mediterranean Ad Hoc Networking Workshop (Med-Hoc-Net ’07)*, Corfu, Greece, June 2007.

[9] A. R. Silva and M. C. Vuran, “Development of a Testbed for Wireless Underground Sensor Networks,” *EURASIP Journal on Wireless Communications and Networking (JWCN)*, vol. 2010, Article ID 620307, 2010.

[10] P. Gupta and P. R. Kumar, “Critical Power for Asymptotic Connectivity,” in *Proc. IEEE CDC*, Tampa, USA, December 1998.

[11] C. Bettstetter, “On the Minimum Node Degree and Connectivity of a Wireless Multihop Network,” in *Proc. ACM MOBIHOC*, Lausanne, Switzerland, June 2002.

[12] C. Bettstetter and C. Hartmann, “Connectivity of Wireless Multihop Networks in a Shadow Fading Environment,” in *ACM-Springer Journal of Wireless Networks (WINET)*, vol.11, no.5, pp. 571-579, 2005.

[13] R. Rajagopalan and P. K. Varshney, “Connectivity Analysis of Wireless Sensor Networks with Regular Topologies in the Presence of Channel Fading,” in *IEEE Trans. on Wireless Communications*, vol.8, no.7, pp. 3475-3483, 2009.

[14] Z. Kong and M. Y. Edmund, “Connectivity and Latency in Large-Scale Wireless Networks with Unreliable Links,” in *Proc. IEEE INFOCOM ’08*, Phoenix, USA, April 2008.

[15] O. Dousse, P. Thiran and M. Hasler, “Connectivity in Ad-Hoc and Hybrid Networks,” in *Proc. IEEE INFOCOM*, New York, June 2002.

[16] O. Dousse, P. Mannersalo, P. Thiran, “Latency of Wireless Sensor Networks with Uncoordinated Power Saving Mechanisms,” in *Proc. ACM MOBIHOC*, Tokyo, Japan, May 2004.

[17] F. Fabbri and R. Verdone, “A Statistical Model for the Connectivity of Nodes in a Multi-Sink Wireless Sensor Network Over a Bounded Region,” in *Proc. European Wireless Conference (EW’08)*, Prague, Czech Republic, June 2008.

[18] A. R. Siva, “Channel Characterization for Wireless Underground Sensor Networks,” *Master of Science Thesis*, University of Nebraska at Lincoln, April 2010. *http://digitalcommons.unl.edu/computerscidiss/13*

[19] T. Camp, J. Boleng and V. Davies, “A Survey of Mobility Models for Ad Hoc Network Research,” *Wireless Communications and Mobile Computing*, vol.2, no.5, pp. 483-502, September 2002.

[20] R. Meester and R. Roy, *Continuum percolation*, Cambridge University Press, 1996.

[21] J. Medhi, *Stochastic processes*, 2nd ed. New York : J. Wiley, 1994.

[22] V. Isham, et.al., “Representation of Space-time Variability of Soil Moisture,” in *Proc. Royal Society*, vol.461, no. 2064, pp. 4035-4055, 2005.

[23] E. Hyytia, P. Lassila and J. Virtamo, "Spatial Node Distribution of the Random Waypoint Mobility Model With Applications," in *IEEE Trans. on Mobile Computing*, Vol. 5, No. 6, pp. 680-694, June 2006.

[24] H. Cai and D. Y. Eun, "Crossing Over the Bounded Domain: From Exponential to Power-law Inter-meeting Time in Mobile Ad-Hoc Networks," in *IEEE/ACM Trans. on Networking*, Vol. 17, No. 5, pp. 1578-1591, October 2009.

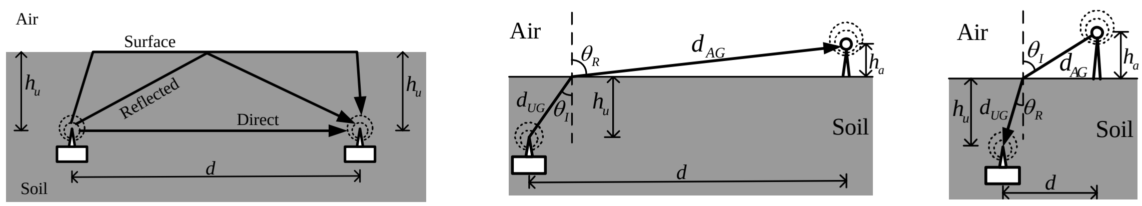

(a) (b) (c)

Fig. 1. Illustration of (1) UG-UG channel, (b) UG-AG channel, and (c) AG-UG channel

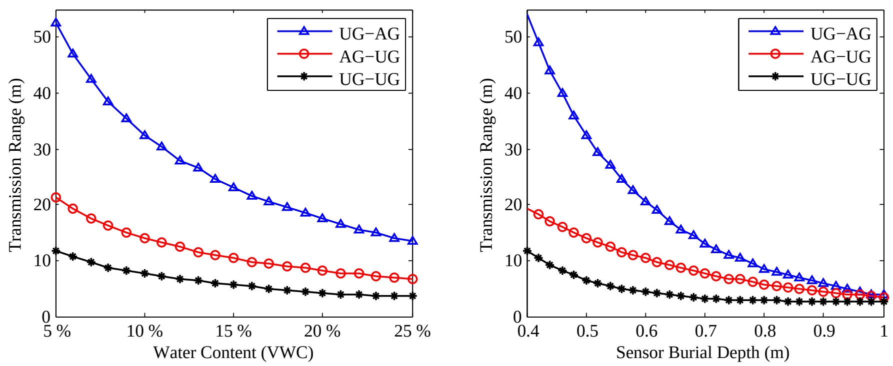

(a) (b)

Fig. 2. Transmission ranges of the three types of channels in WUSNs as functions of (a) volumetric water content and (b) sensor burial depth.

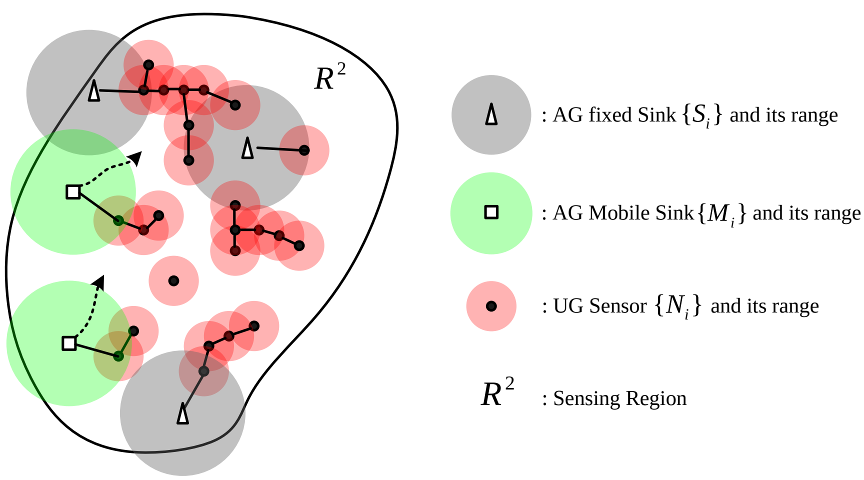

Fig. 3. The network model of the WUSNs.

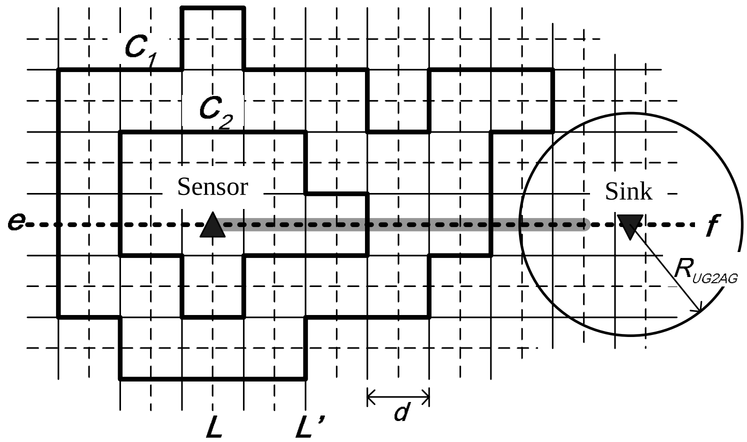

Fig. 4. Mapping the WUSN on a lattice **L** (dashed) and its dual **L'** (plain).

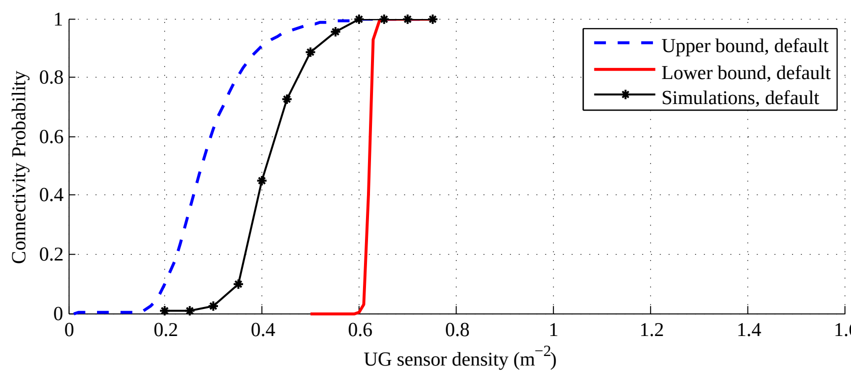

Fig. 5. Connectivity probability in WUSNs as a function of UG sensor node density with default system and environmental parameters.

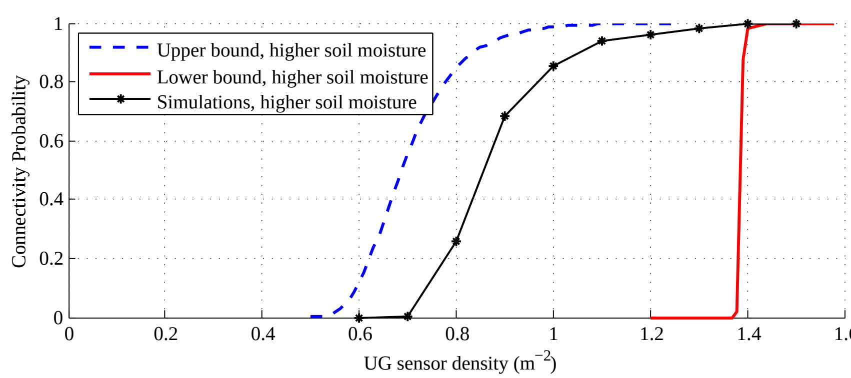

Fig. 6. Connectivity probability in WUSNs as a function of UG sensor node density in soil medium with higher soil moisture (VWC=22%).

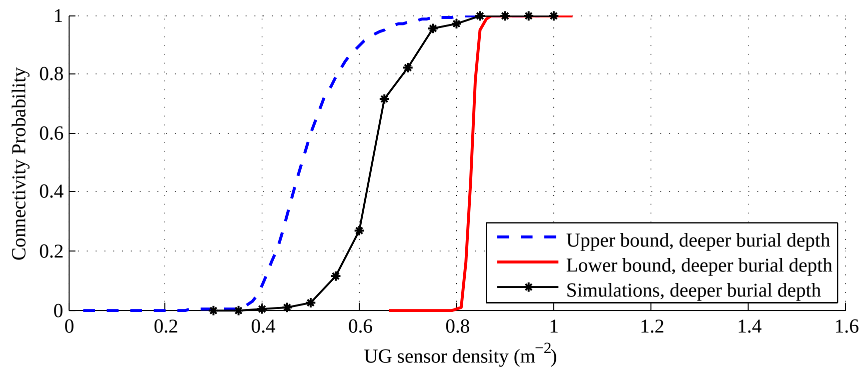

Fig. 7. Connectivity probability in WUSNs as a function of UG sensor node density with deeper sensor burial depth (mean depth is 1 m).

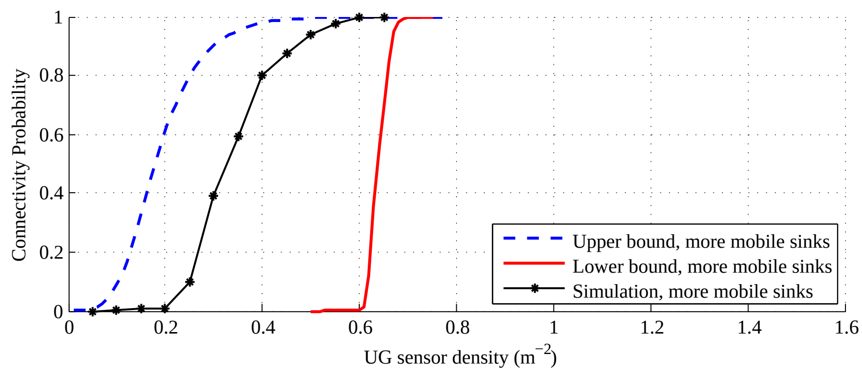

Fig. 8. Connectivity probability in WUSNs as a function of UG sensor node density with four times more AG mobile sinks ($m = 50$).

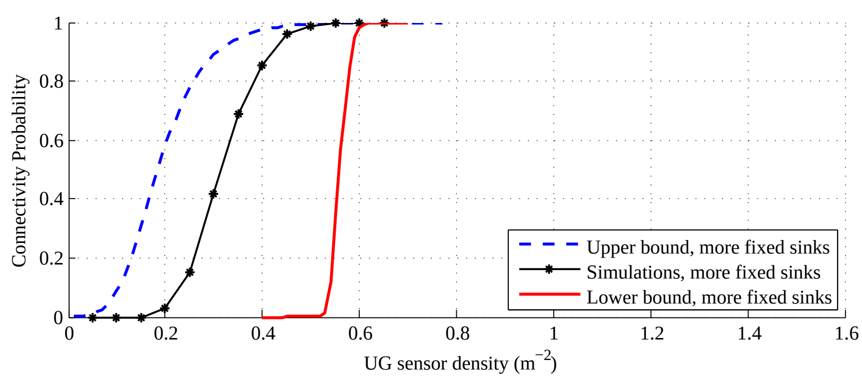

Fig. 9. Connectivity probability in WUSNs as a function of UG sensor node density with two times AG fixed sink density ($\lambda_a = 0.002\ m^{-2}$).

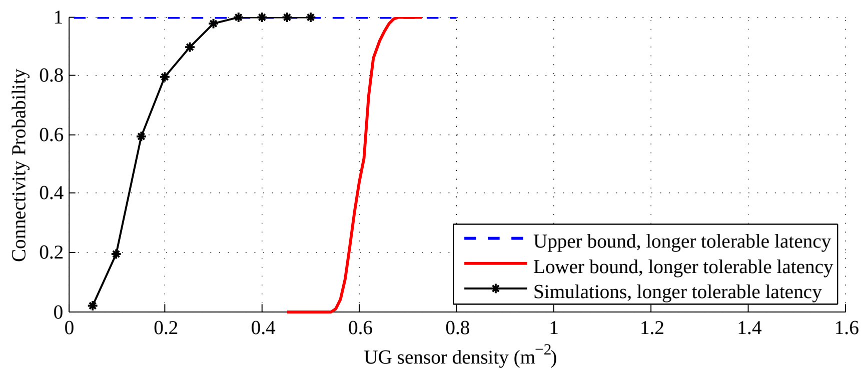

Fig. 10. Connectivity probability in WUSNs as a function of UG sensor node density with longer tolerable latency (t_s = 300 sec).

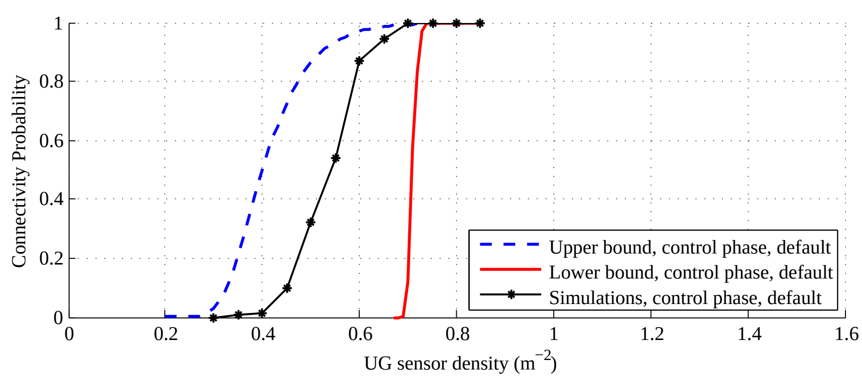

Fig. 11. Connectivity probability in WUSNs as a function of UG sensor node density in control phase with default parameters.